Surface-State-Dominated Spin-Charge Current Conversion in Topological-Insulator–Ferromagnetic-Insulator Heterostructures

Hailong Wang,[1] James Kally,[1] Joon Sue Lee,[1] Tao Liu,[2] Houchen Chang,[2] Danielle Reifsnyder Hickey,[3]
K. Andre Mkhoyan,[3] Mingzhong Wu,[2] Anthony Richardella,[1] and Nitin Samarth[1,*]

[1]*Department of Physics, The Pennsylvania State University, University Park, Pennsylvania 16802, USA*
[2]*Department of Physics, Colorado State University, Fort Collins, Colorado 80523, USA*
[3]*Department of Chemical Engineering and Materials Science, University of Minnesota, Minneapolis, Minnesota 55455, USA*

We report the observation of ferromagnetic resonance-driven spin pumping signals at room temperature in three-dimensional topological insulator thin films—Bi_2Se_3 and $(Bi, Sb)_2Te_3$—deposited by molecular beam epitaxy on $Y_3Fe_5O_{12}$ thin films. By systematically varying the Bi_2Se_3 film thickness, we show that the spin-charge conversion efficiency, characterized by the inverse Rashba-Edelstein effect length (λ_{IREE}), increases dramatically as the film thickness is increased from two quintuple layers, saturating above six quintuple layers. This suggests a dominant role of surface states in spin and charge interconversion in topological-insulator–ferromagnet heterostructures. Our conclusion is further corroborated by studying a series of $Y_3Fe_5O_{12}/(Bi, Sb)_2Te_3$ heterostructures. Finally, we use the ferromagnetic resonance linewidth broadening and the inverse Rashba-Edelstein signals to determine the effective interfacial spin mixing conductance and λ_{IREE}.

The development of next-generation spintronic devices has driven extensive studies of spin-to-charge conversion through measurements of the inverse spin Hall effect (ISHE) and/or the inverse Rashba-Edelstein effect (IREE) in both three-dimensional (3D) [1–6] and two-dimensional (2D) material systems [7–15]. Topological insulators (TIs) such as the Bi-chalcogenides are naturally relevant in this context due to the large spin-orbit coupling (SOC) strength and the inherent spin-momentum "locking" in their surface states [9,16,17] which promise very efficient spin-charge conversion. Previous studies of spin transfer in TI-based heterostructures have involved ferromagnetic metals that provide a shunting current path, therefore introducing potential artifacts which complicate the picture and analysis [8,9,11,12]. To circumvent these problems, we have grown and characterized bilayers of TIs on ferrimagnetic insulator $Y_3Fe_5O_{12}$ (YIG) thin films with an exceptionally low damping constant [18]. Here, we report the ferromagnetic resonance (FMR)-driven spin pumping observed in YIG/Bi_2Se_3 bilayers, showing robust spin pumping signals at room temperature. Systematic variation of the Bi_2Se_3 thickness allows us to unambiguously demonstrate that the spin-charge conversion efficiency, characterized by the inverse Rashba-Edelstein effect length λ_{IREE} in a 2D material system [7], dramatically increases from (1.1 ± 0.13) pm to 35 ± 4 pm as the Bi_2Se_3 thickness varies from 2 to 6 quintuple layers (QL). When the top and bottom surface states with opposite spin polarizations decouple from each other, λ_{IREE} saturates and is constant, providing clear evidence for the dominant role of surface states in inducing spin-charge conversion in 3D TIs.

We first discuss the structural and interfacial characterization of the YIG/Bi_2Se_3 heterostructure using high-resolution scanning transmission electron microscopy (HR-STEM). Figure 1(a) shows an atomically ordered 6 QL Bi_2Se_3 layer grown on an epitaxial 30-nm YIG thin film. We note that an amorphous layer of about 1 nm in thickness is observed at the YIG/Bi_2Se_3 interface, most likely due to the nucleation of the template layer in the two-step growth process (see Supplemental Material [19] for more details about the growth method). The atomic force microscopy image in Fig. 1(b) shows a smooth surface with a roughness of about 0.71 nm. A representative $\theta - 2\theta$ x-ray diffraction (XRD) scan of a 40 QL Bi_2Se_3 film shown in Fig. 1(c) indicates a phase-pure Bi_2Se_3 layer. Figure 1(d) shows a representative FMR derivative absorption spectrum for a 30-nm YIG film used in this study taken at a radio-frequency (rf) $f = 3$ GHz with a magnetic field H applied in the film plane. The peak-to-peak line width (ΔH_{PP}) obtained from the spectrum is 9.2 Oe, and an effective saturation induction of 1.76 kOe is extracted from fitting the frequency dependence of the resonance field [18]. The spin pumping measurements are performed using a microwave transmission line on the YIG/TI bilayers at room temperature (approximate sample dimensions of 1 mm × 5 mm). During the measurements, a dc magnetic field H is applied in the $x - z$ plane and the spin pumping voltage V_{SP} is measured across the ~5 mm long TI layer along the y axis, as illustrated in Fig. 2(a). At the resonance condition, the YIG magnetization M precesses around the equilibrium position and transfers angular momentum to the conduction electrons in the TI films through interfacial
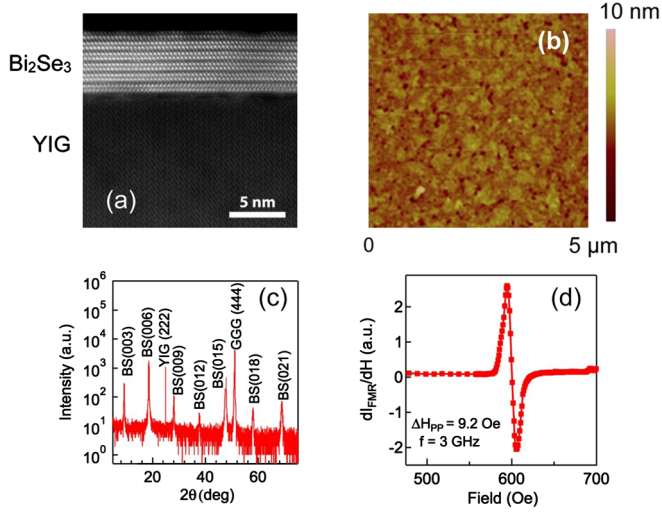
FIG. 1.   (a) Cross-sectional high-angle annular dark-field scanning TEM image of the YIG/Bi_2Se_3 interface. (b) Atomic force microscopy image of the YIG/Bi_2Se_3 (6 QL) sample with a surface roughness of 0.71 nm. (c) Semilog $\theta - 2\theta$ XRD scan of a YIG/Bi_2Se_3 (40 QL) sample which exhibits clear x-ray scattering peaks from the (003) to (0021) planes of Bi_2Se_3. (d) A representative room-temperature FMR derivative spectrum of a 30-nm YIG film with an in-plane field, which gives a peak-to-peak line width of 9.2 Oe at $f = 3$ GHz.

FIG. 2.   (a) Schematic of the experimental setup for FMR spin pumping measurements. (b) Resistivity of 6 QL Bi_2Se_3 and $(Bi, Sb)_2Te_3$ thin films grown on YIG as a function of temperature. (c) V_{SP} vs H spectra of YIG/Bi_2Se_3 (6 QL) at $f = 2, 3,$ and 4 GHz using 100 mW microwave power. (d) V_{SP} vs H spectra of the YIG/Bi_2Se_3 (6 QL) sample for the microwave power of 18, 32, 56, and 100 mW (blue, black, green, red curves, respectively) at $f = 3$ GHz. Inset: rf power dependence of the corresponding V_{SP} at $\theta_H = 90°$.

exchange coupling [4]. The resulting pure spin current is injected along the z axis with spin polarization σ parallel to M, and then converted to a charge current leading to the spin pumping signal.

Figure 2(b) shows the temperature dependence of the resistivity of 6 QL Bi_2Se_3 and $(Bi, Sb)_2Te_3$ thin films grown on YIG. The metallic behavior (decrease in resistivity at low temperature) is the typical behavior of Bi_2Se_3 due to Se vacancies [20]. For $(Bi, Sb)_2Te_3$, the resistivity increases by ~50% from room temperature to 2 K, consistent with surface state dominated transport in this thin film [21]. The carrier concentrations obtained from Hall effect measurements at room temperature are 4×10^{13} cm^{-2} and 9.8×10^{12} cm^{-2} for 6 QL Bi_2Se_3 and $(Bi, Sb)_2Te_3$, respectively.

Figure 2(c) shows the observed V_{SP} vs H spectra of the YIG/Bi_2Se_3 (6QL) bilayers at $f = 2, 3,$ and 4 GHz using 100 mW microwave power. The observed spin pumping signals change sign when the magnetic field H is reversed from $\theta_H = 90°$ to $270°$, as expected from either IREE or ISHE. At 2 and 3 GHz, the observed signal is about 40 μV, and for 4 GHz, the signal decreases to about 20 μV, which results from the variation of the microwave transmission line performance at different frequencies. Figure 2(d) shows the spin pumping spectra of a YIG/Bi_2Se_3 (6 QL) sample at microwave powers of 18, 32, 56, and 100 mW and an excitation frequency of 3 GHz. The upper inset shows the rf power dependence of V_{SP} at $\theta_H = 90°$, indicating that the observed spin pumping signals are in the linear regime.
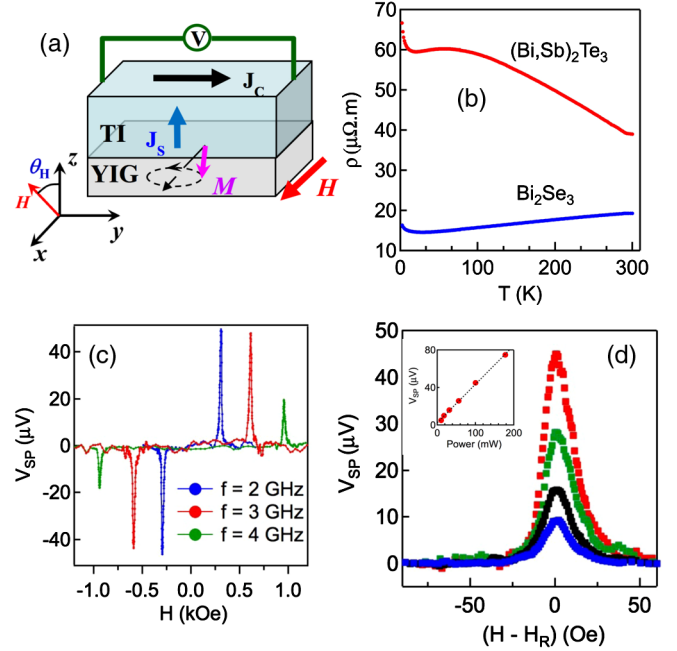
To probe the spin-to-charge conversion mechanism in TI layers, we systematically vary the Bi_2Se_3 thickness from 2 to 60 QL. Figure 3(a) shows the spin pumping spectra when $\theta_H = 90°$ for 4, 6, 24, and 40 QL thicknesses of Bi_2Se_3 grown on YIG, respectively. The significant enhancement of the spin pumping signal in the low Bi_2Se_3 thickness regime mainly results from the increased resistivity. For a 2D material system, such as the TI surface states, the spin-to-charge conversion is dominated by IREE [21,22] and the injected spin current is converted into a 2D charge current, $J_c = \lambda_{IREE}J_s$. The spin current density J_s is in units of A m^{-2}, and the 2D charge current density J_c is in units of A m^{-1}; the parameter λ_{IREE} has the dimension of length and is introduced to characterize the spin-to-charge conversion efficiency in 2D material systems [7,23]. The observed spin pumping voltages V_{SP} dominated by IREE depend on several material parameters [7]:

$$V_{SP} = -wR\lambda_{IREE}J_s, \qquad (1)$$

where w and R are the sample width and resistance, respectively. J_s is the spin current density at the YIG/TI interface which can be expressed as [3,5,6]

$$J_s = \frac{2e}{\hbar} \frac{g_{\uparrow\downarrow} h_{rf}^2 \hbar \omega^2 [\gamma 4\pi M_s + \sqrt{(\gamma 4\pi M_s)^2 + 4\omega^2}]}{2\pi (\Delta H_{pp})^2 [(\gamma 4\pi M_s)^2 + 4\omega^2]}, \qquad (2)$$
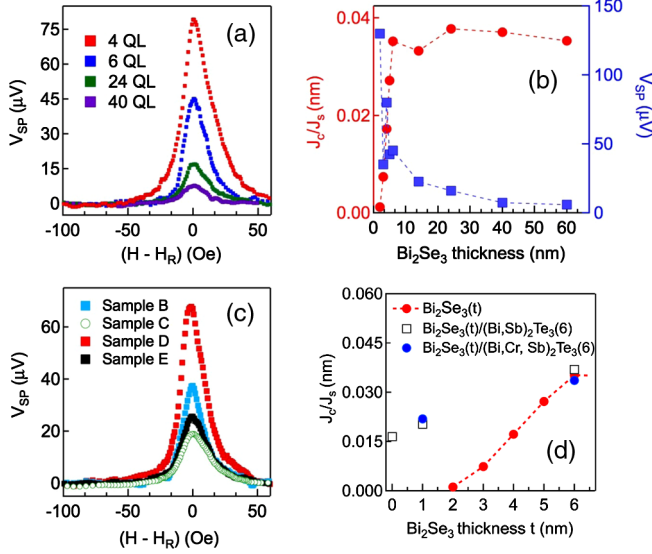
FIG. 3. (a) V_{SP} vs H spectra of YIG/Bi$_2$Se$_3$ (4 QL), YIG/Bi$_2$Se$_3$ (6 QL), YIG/Bi$_2$Se$_3$ (24 QL), and YIG/Bi$_2$Se$_3$ (40 QL) at $f = 3$ GHz using 100 mW microwave power. The x axis is shifted by the resonance field (H_R) for clarity. (b) Dependence of V_{SP} (blue points) and the spin-to-charge conversion efficiency J_c/J_s determined by λ_{IREE} (red points) on the Bi$_2$Se$_3$ thickness. (c) V_{SP} vs H spectra of control sample B: YIG/Bi$_2$Se$_3$(1QL)/(Bi, Sb)$_2$Te$_3$(6QL) (blue curve); sample C: YIG/Bi$_2$Se$_3$(6QL)/(Bi, Sb)$_2$Te$_3$(6QL) (green curve); sample D: YIG/Bi$_2$Se$_3$(1QL)/Cr$_{0.2}$(Bi$_{0.5}$Sb$_{0.5}$)$_{1.8}$Te$_3$(6QL) (red curve), and sample E: YIG/Bi$_2$Se$_3$(6QL)/Cr$_{0.2}$(Bi$_{0.5}$Sb$_{0.5}$)$_{1.8}$Te$_3$(6QL) (black curve) at 3 GHz and 100 mW. (d) Comparison of J_c/J_s for the control samples with the corresponding values for YIG/Bi$_2$Se$_3$.

where $g_{\uparrow\downarrow}$ is the effective interfacial spin mixing conductance [24], ΔH_{pp} is the FMR peak-to-peak linewidth, h_{rf} is the radio-frequency field, ω is the FMR angular frequency, and M_s is the saturation induction of the YIG thin films. We can determine the effective spin mixing conductance $g_{\uparrow\downarrow}$ from the FMR linewidth broadening of the YIG thin film [2,3,24]:

$$g_{\uparrow\downarrow} = \frac{2\pi\sqrt{3}M_s\gamma t_{YIG}}{g\mu_B\omega}(\Delta H_{YIG/TI} - \Delta H_{YIG}), \quad (3)$$

where γ is the absolute gyromagnetic ratio, t_{YIG} denotes the thickness of the YIG thin films, g is the Landé factor, and μ_B is the Bohr magnetron.

If the spin pumping signal is dominated by the ISHE, spin diffusion should be taken into account according to $J_c = \theta_{SH}\lambda_{SD}\tanh[t_{TI}/(2\lambda_{SD})]J_s$, and the spin pumping signal will follow [2,3,6]:

$$V_{SP} = -wR\theta_{SH}\lambda_{SD}\tanh\left(\frac{t_{TI}}{2\lambda_{SD}}\right)J_s, \quad (4)$$

where λ_{SD} is the spin diffusion length, t_{TI} is the thickness of the TI thin film and θ_{SH} is the spin Hall angle. The distinct

difference between Eqs. (1) and (4) is whether the observed spin pumping signal is dominated by the spin momentum "locking" in the surface states [25–27] or by the SOC interaction.

To answer this question, Fig. 3(b) shows the Bi$_2$Se$_3$ thickness dependence of V_{SP} (blue points) and λ_{IREE} (or J_c/J_s) (red points), where we define $J_c = (V_{SP}/wR)$. Above 6 QL, J_c/J_s almost follows a constant value of about 35 pm. Below 6 QL, J_c/J_s dramatically decays by a factor of 30 from 35 ± 4 pm to 1.1 ± 0.13 pm when at 2 QL thickness. Earlier studies have reported that the thickness of the Bi$_2$Se$_3$ surface states is approximately 2–3 nm [28,29]. Above 6 QL, the top and bottom Bi$_2$Se$_3$ surface states decouple from each other; below 6 QL, the interaction of the two surface states with opposite spin polarizations can decrease the interfacial spin momentum "locking" efficiency. This is consistent with angle-resolved photoemission spectroscopy studies that show the opening of a gap in the Dirac cone when the Bi$_2$Se$_3$ thickness is below 6 QL, accompanied by a decrease in the spin polarization of the surface states [28,29]. Qualitatively, our data shown in Fig. 3(b) follow this trend and strongly indicate the key role played by the surfaces states in spin-charge conversion in Bi$_2$Se$_3$. If we try to interpret the data in Fig. 3(b) with the spin diffusion model [Eq. (4)], the fit yields a value of $\lambda_{SD} \sim 1.6$ nm and also requires the presence of a "dead" layer at the interface (see Supplemental Material [19] for detailed analysis using the spin diffusion model). This short vertical spin diffusion length suggests that the spin polarized electron current is restricted to the bottom surface of the TI. Thus, while we cannot definitively rule out the spin diffusion model, a more physically meaningful picture at this stage is that the surface states probably play a dominant role in the spin-charge conversion. We note that the value we obtain for (J_c/J_s) (or λ_{IREE}) is approximately 2 orders of magnitude smaller than the spin Hall angle reported using a spin torque FMR study at room temperature [9]. One possible reason for this discrepancy is the amorphous layer at the interface shown in the HR-STEM figure, which potentially decreases the spin injection efficiency. Another reason may be the difference in the fundamental measurement mechanism between these two probing techniques. In a spin torque FMR experiment, as the charge current flows through the TI layers, the electrons can potentially have multiple scattering processes to transfer the spins to the ferromagnetic layers. However, in an FMR spin pumping measurement, this multiple scattering process may not be valid.

To further verify that the spin-charge conversion efficiency is dominated by the surface states of TIs, we grew five different TI heterostructures on YIG as control samples and measured their spin pumping signals. The five control samples are sample A: YIG/(Bi, Sb)$_2$Te$_3$ (6 QL); sample B: YIG/Bi$_2$Se$_3$ (1 QL)/(Bi, Sb)$_2$Te$_3$ (6 QL); sample C: YIG/Bi$_2$Se$_3$ (6 QL)/(Bi, Sb)$_2$Te$_3$ (6 QL); sample D:

YIG/Bi_2Se_3 (1 QL)/$Cr_{0.2}(Bi_{0.5}Sb_{0.5})_{1.8}Te_3$ (6 QL);   and
sample   E: YIG/Bi_2Se_3 (6 QL)/$Cr_{0.2}(Bi_{0.5}Sb_{0.5})_{1.8}$
Te_3 (6 QL). Figure 3(c) shows the spin pumping spectra
of control samples B, C, D, and E at 3 GHz radio-
frequency and 100 mW power. The enhancement of the
spin pumping signal of samples D and E mainly results
from the larger resistivity of $Cr_{0.2}(Bi_{0.5}Sb_{0.5})_{1.8}Te_3$ com-
pared to $(Bi, Sb)_2Te_3$. Normalizing by the resistance and
sample width, we obtained the spin charge conversion
ratio of the five control samples and compared them with
the values for YIG/Bi_2Se_3 in Fig. 3(d). First, the values of
λ_{IREE} obtained for sample C and sample E are 37 ± 4 pm
and 34 ± 4 pm, respectively. Both the values are quite
close to 35 ± 4 pm measured for YIG/Bi_2Se_3 (6 QL),
indicating that as long as the Bi_2Se_3 thickness is above
6 QL, the spin-charge conversion efficiency is roughly
constant and does not depend on the bulk properties: Cr
doping and different band structures do not change the
values. Second, for sample A, $(Bi, Sb)_2Te_3$ directly grown
on YIG, $\lambda_{IREE} = 17 \pm 2$ pm, about half of the value of
Bi_2Se_3. This is in sharp contrast with earlier results which
reported a much larger spin Hall angle of the $(Bi, Sb)_2Te_3$
compared with Bi_2Se_3 using a spin-polarized tunneling
study [23]. This most likely results from the different
interfacial quality and conditions that determine the spin
momentum "locking" efficiency. We expect that the bottom
surface state condition at the YIG/$(Bi, Sb)_2Te_3$ interface
[28] is not as good as the CoFeB/MgO/$(Bi, Sb)_2Te_3$
interface [23] for which TI was grown on the commercial
InP substrates with minimal lattice mismatch and the highest
sample quality. In the end, we compare the values in samples
B and D that both have 1 QL Bi_2Se_3 seed layers. For sample
D, we intentionally dope the $(Bi, Sb)_2Te_3$ with Cr, which
can induce ferromagnetism at low temperature [30,31]. At
room temperature, the Cr doping mainly changes the trans-
port properties and the SOC strength of the bulk states. The
values for samples B and D are $\lambda_{IREE} = 20 \pm 2$ pm and
22 ± 3 pm, respectively. Their similar spin-charge conver-
sion efficiencies demonstrate that the properties of the TI
bulk state do not play a significant role here, confirming the
interface-dominated spin pumping phenomena. It is also
important to note that values of λ_{IREE} for samples B and D are
lower than the value for YIG/Bi_2Se_3 (6 QL). As in other
studies of spin pumping into TIs, the interfacial condition
presents a critical challenge for controlling the spin con-
version efficiency [8,11,12]; in sample B, both YIG/Bi_2Se_3
and Bi_2Se_3/$(Bi, Sb)_2Te_3$ interfaces will contribute to the
formation of the surface states. Thus, structural defects
and/or strain induced dislocations in the trilayer hetero-
structures can potentially result in the observed lower
values. A thorough understanding about the correlation of
the interfacial conditions of TI surfaces states and the spin-
charge conversion efficiency requires further investigation.

Finally, we compare the spin transfer efficiency at
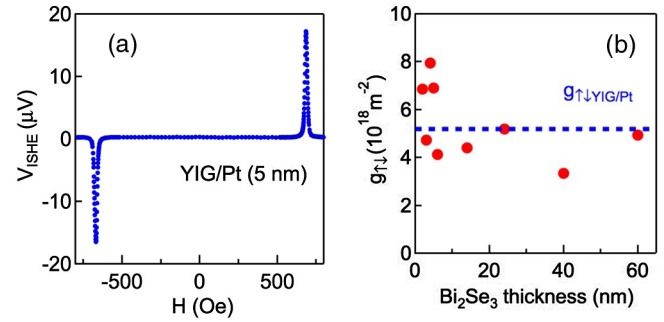YIG/Bi_2Se_3 to that at YIG/Pt. Note that Pt is an ideal

FIG. 4.   (a) V_{ISHE} vs H spectra of YIG/Pt (5 nm) bilayer at
radio-frequency of 3 GHz and 100 mW microwave power.
(b) Dependence of the YIG/Bi_2Se_3 interfacial spin mixing
conductance $g_{\uparrow\downarrow}$ on Bi_2Se_3 thickness. The blue dashed line
indicates the value of $g_{\uparrow\downarrow}$ at the YIG/Pt interface.

spin sink and a well-studied nonmagnetic material with large
SOC [3,6]. Figure 4(a) shows the inverse spin Hall spectrum
of a YIG(30 nm)/Pt (5 nm) bilayer sample under 3 GHz
and 100 mW microwave power when the H field is in plane.
The observed sign change of the spin pumping signal with
field reversal is expected for the ISHE in a 3D material
system [2,3]. From the FMR linewidth broadening, the
obtained YIG/Pt effective spin mixing conductance is
$(5.19 \pm 0.6) \times 10^{18}$ m^{-2}, which lies in the range of the
values reported by other groups using spin pumping [5,6].
We compare this value with the obtained spin mixing
conductance at various Bi_2Se_3 thicknesses in Fig. 4(b).
When Bi_2Se_3 is 6 QL thick, the spin mixing conductance
at the YIG/Bi_2Se_3 interface is $(4.13 \pm 0.5) \times 10^{18}$ m^{-2}.
Although there are some variations, the reported values are
in the range of $3–7 \times 10^{18}$ m^{-2} when the Bi_2Se_3 thickness
varies from 2 to 60 QL, which is essentially comparable to
the determined value at the YIG/Pt interface, demonstrating
an efficient spin transfer in YIG/TI heterostructures. It is
important to note that in the large Bi_2Se_3 thickness
regime, we do not observe an enhancement of $g_{\uparrow\downarrow}$, which
is typically observed in the YIG/transition metal bilayers
due to the decrease in backflow spin current caused by
the spin diffusion in the bulk [24,32]. This also confirms
the TI surface states dominated spin-charge conversion
mechanism.

In conclusion, we report robust spin pumping at room
temperature in YIG/Bi_2Se_3 bilayers and other YIG/TI
heterostructures. By measuring IREE voltages and inter-
facial spin current density, we determine the value of λ_{IREE}
and reveal its systematic behavior with Bi_2Se_3 thickness,
demonstrating the dominant role of surface states in spin-
charge conversion. The inferred IREE length indicates the
important role of interface conditions in spin Hall physics
in topological insulators. Further investigation is required
for a thorough understanding of the correlation between the
formation of the surface states and the variation of spin-
charge conversion efficiency at the interfaces.

Note added in proof.—Recently, we became aware of a recent experiment that uses the spin Seebeck effect to demonstrate spin-charge conversion in similar topological-insulator-ferromagnetic insulator heterostructures [33].

---

*nsamarth@psu.edu

[1] Y. Kajiwara, K. Harii, S. Takahashi, J. Ohe, K. Uchida, M. Mizuguchi, H. Umezawa, H. Kawai, K. Ando, K. Takanashi, S. Maekawa, and E. Saitoh, Nature (London) **464,** 262 (2010).

[2] B. Heinrich, C. Burrowes, E. Montoya, B. Kardasz, E. Girt, Y.-Y. Song, Y. Y. Sun, and M. Z. Wu, Phys. Rev. Lett. **107,** 066604 (2011).

[3] O. Mosendz, V. Vlaminck, J. E. Pearson, F. Y. Fradin, G. E. W. Bauer, S. D. Bader, and A. Hoffmann, Phys. Rev. B **82,** 214403 (2010).

[4] C. H. Du, H. L. Wang, Y. Pu, T. L. Meyer, P. M. Woodward, F. Y. Yang, and P. C. Hammel, Phys. Rev. Lett. **111,** 247202 (2013).

[5] C. Hahn, G. de Loubens, O. Klein, M. Viret, V. V. Naletov, and J. Ben Youssef, Phys. Rev. B **87,** 174417 (2013).

[6] H. L. Wang, C. H. Du, Y. Pu, R. Adur, P. C. Hammel, and F. Y. Yang, Phys. Rev. Lett. **112,** 197201 (2014).

[7] J. C. Rojas Sánchez, L. Vila, G. Desfonds, S. Gambarelli, J. P. Attané, J. M. De Teresa, C. Magén, and A. Fert, Nat. Commun. **4,** 2944 (2013).

[8] Y. Shiomi, K. Nomura, Y. Kajiwara, K. Eto, M. Novak, K. Segawa, Y. Ando, and E. Saitoh, Phys. Rev. Lett. **113,** 196601 (2014).

[9] A. R. Mellnik, J. S. Lee, A. Richardella, J. L. Grab, P. J. Mintun, M. H. Fischer, A. Vaezi, A. Manchon, E.-A. Kim, N. Samarth, and D. C. Ralph, Nature (London) **511,** 449 (2014).

[10] Y. Fan, P. Upadhyaya, X. Kou, M. Lang, S. Takei, Z. Wang, J. Tang, L. He, L.-T. Chang, M. Montazeri, G. Yu, W. Jiang, T. Nie, R. N. Schwartz, Y. Tserkovnyak, and K. L. Wang, Nat. Mater. **13,** 699 (2014).

[11] P. Deorani, J. Son, K. Banerjee, N. Koirala, M. Brahlek, S. Oh, and H. Yang, Phys. Rev. B **90,** 094403 (2014).

[12] M. Jamali, J. S. Lee, J. S. Jeong, F. Mahfouzi, Y. Lv, Z. Zhao, B. K. Nikolic, K. A. Mkhoyan, N. Samarth, and J.-P. Wang, Nano Lett. **15,** 7126 (2015).

[13] A. A. Baker, A. I. Figueroa, L. J. Collins-McIntyre, G. van der Laan, and T. Hesjedal, Sci. Rep. **5,** 7907 (2015).

[14] Y. Wang, P. Deorani, K. Banerjee, N. Koirala, M. Brahlek, S. Oh, and H. Yang, Phys. Rev. Lett. **114,** 257202 (2015).

[15] K. Kondou, R. Yoshimi, A. Tsukazaki, Y. Fukuma, J. Matsuno, K. S. Takahashi, M. Kawasaki, Y. Tokura, and Y. Otani, Nat. Phys., doi:10.1038/nphys3833 (2016).

[16] D. Hsieh et al., Nature (London) **460,** 1101 (2009).

[17] M. Z. Hasan and C. L. Kane, Rev. Mod. Phys. **82,** 3045 (2010).

[18] H. Chang, P. Li, W. Zhang, T. Liu, A. Hoffmann, L. Deng, and M. Wu, IEEE Magn. Lett. **5,** 6700104 (2014).

[19] See Supplemental Material at http://link.aps.org/supplemental/10.1103/PhysRevLett.117.076601 for detailed information of topological insulators growth and spin current analysis.

[20] A. Kandala, A. Richardella, D. W. Rench, D. M. Zhang, T. C. Flanagan, and N. Samarth, Appl. Phys. Lett. **103,** 202409 (2013).

[21] J. S. Lee, A. Richardella, D. Reifsnyder Hickey, K. A. Mkhoyan, and N. Samarth, Phys. Rev. B **92,** 155312 (2015).

[22] V. M. Edelstein, Solid State Commun. **73,** 233 (1990).

[23] K. Shen, G. Vignale, and R. Raimondi, Phys. Rev. Lett. **112,** 096601 (2014).

[24] Y. Tserkovnyak, A. Brataas, G. E. W. Bauer, and B. I. Halperin, Rev. Mod. Phys. **77,** 1375 (2005).

[25] L. Liu, A. Richardella, I. Garate, Y. Zhu, N. Samarth, and C.-T. Chen, Phys. Rev. B **91,** 235437 (2015).

[26] J. Tang, L.-T. Chang, X. Kou, K. Murata, E. S. Choi, M. Lang, Y. Fan, Y. Jiang, M. Montazeri, W. Jiang, Y. Wang, L. He, and K. L. Wang, Nano Lett. **14,** 5423 (2014).

[27] C. H. Li, O. M. J. van't Erve, J. T. Robinson, Y. Liu, L. Li, and B. T. Jonker, Nat. Nanotechnol. **9,** 218 (2014).

[28] Y. Zhang et al., Nat. Phys. **6,** 584 (2010).

[29] M. Neupane et al., Nat. Commun. **5,** 3841 (2014).

[30] Z. Jiang, C.-Z. Chang, C. Tang, P. Wei, J. S. Moodera, and J. Shi, Nano Lett. **15,** 5835 (2015).

[31] A. Kandala, A. Richardella, S. Kempinger, C.-X. Liu, and N. Samarth, Nat. Commun. **6,** 7434 (2015).

[32] H. J. Jiao and G. E. W. Bauer, Phys. Rev. Lett. **110,** 217602 (2013).

[33] Z. Jiang, C.-Z. Chang, M. R. Masir, C. Tang, Y. Xu, J. S. Moodera, A. H. MacDonald, and J. Shi, Nat. Commun. **7,** 11458 (2016)